ISIJ International, Vol. 61 (2021), No. 6, pp. 1775–1783
https://doi.org/10.2355/isijinternational.ISIJINT-2020-688

# Effect of Impeller and Gas Stirring on Agglomeration Behavior of Polydisperse Fine Particles in Liquid

Akito YAMAGUCHI,[1)] Hitoshi OKANO,[2)] Syunsuke SUMITOMO,[3)] Md. Azhar UDDIN[1)] and Yoshiei KATO[1)]*

1) Department of Material and Energy Science, Graduate School of Environmental and Life Science, Okayama University, 1-1 Tsushima-naka, 3-chome, Kita-ku, Okayama, 700-8530 Japan.
2) Department of Material and Energy Science, Graduate School of Environmental Science, Okayama University. Now at Nihon Tokushu Rozai Co. Ltd., 4-1, Chikko, 5-chome, Tamano, 706-0002 Japan.
3) Department of Material and Energy Science, Graduate School of Environmental and Life Science, Okayama University. Now at Kagawa Prefectural Environmental Health Research Center, 3-105, Asahi-cho, 5-chome, Takamatsu, 760-0065 Japan.

(*Received on November 10, 2020; accepted on February 24, 2021*)

Agglomeration, coalescence and flotation of non-metallic inclusions in steel melt are effective for obtaining "clean steel." In this study, the agglomeration and breakup behaviors of particles with a primary particle size distribution (hereinafter, polydisperse particles) in a liquid under impeller and gas stirring were compared by numerical calculations and model experiments. The particle-size-grouping (PSG) method in the numerical agglomeration model of particles was combined with a breakup term of agglomeration due to bubble bursting at the free surface. Polydisperse and monodisperse polymethylmethacrylate (PMMA) particles were used in the agglomeration experiments. The agglomeration rate of the polydisperse particles under impeller stirring was increased by an increasing energy input rate, whereas the agglomeration rate under gas stirring decreased under this condition due to the larger contribution of the breakup of agglomerated particles during bubble bursting in gas stirring. At the same energy input rate, agglomeration of polydisperse particles was larger under impeller stirring than under gas stirring. The agglomeration rate of polydisperse particles was larger than that of monodisperse particles under both impeller and gas stirring at the same energy input rate. The computational temporal changes in the total number of particles were in good agreement with the experimental results. This means that the difference in the agglomeration behaviors observed in impeller and gas stirring can be explained by the turbulent coagulation and subsequent agglomerated particle breakup in gas stirring. The computational temporal change in the number of each group approximately agreed with the experimental change in both impeller and gas stirring.

KEY WORDS: agglomeration; breakup; particle; impeller stirring; gas agitation; particle-size-grouping method.

## 1. Introduction

Non-metallic inclusions composed of fine oxide particles mainly derive from the deoxidation of the steel melt and entrainment of slag during the steelmaking process, and must be removed as much as possible to prevent deterioration of steel product quality. Non-metallic inclusions in a steel melt are reduced in the secondary refining process and the continuous casting tundish. Agglomeration and flotation of inclusion particles are effective for removing non-metallic inclusions and obtaining "clean steel."

Based on this perspective, many numerical and experimental studies on non-metallic inclusion removal have been carried out covering an induction furnace,[1,2)] gas stirring in a ladle,[3,4)] RH degassing[5,6)] and a continuous casting tundish[7–12)] and mold,[13)] among others. As a pioneering work in this field, Lindborg and Torssell[14)] applied a population balance model[15)] of inclusion growth and removal to explain their experimental study. Cold model experiments with theoretical analyses have also been done to understand the agglomeration behavior of fine particles, particularly the particle collision frequency in a turbulent flow,[16–18)] the heterogeneous agglomeration behavior of two types of fine particles with different surface electrifications and sizes,[19–23)] agglomeration of polydisperse fine particles of the same kind[24–26)] and breakup of agglomerated particles due to collision and fluid shear stress.[27–30)]

Many of these studies treat the agglomeration behavior under a turbulent flow field introduced by Saffman and Turner.[31)] The turbulent energy dissipation rate (= energy

* Corresponding author: E-mail: y-kato@cc.okayama-u.ac.jp

input rate) was associated with the agglomeration rate. Sumitomo *et al.*[32] carried out agglomeration experiments with monodisperse polymethylmethacrylate (PMMA) particles and reported that the agglomeration rate in a gas stirring process was less than that under impeller stirring at the same energy input rate. They explained this difference by noting that part of the agglomerated particles adhering to the floating bubble surface broke up during bubble bursting at the liquid free surface. However, they did not compare the agglomeration behavior of polydisperse particles in different types of stirring processes, although there was a size distribution of the non-metallic inclusion in the steel melt before the removal operation.[33,34] Nakaoka *et al.*[24] developed a particle-size-grouping (PSG) method and successfully applied it to the turbulent agglomeration behavior of particles during impeller stirring.

Targeting a comparison of the PMMA agglomeration behavior in impeller stirring and gas stirring processes, in the present study, agglomeration experiments were carried out with polydisperse particles as well as monodisperse ones. A combination model of the agglomeration and breakup behavior of PMMA particles with an initial size distribution was developed by combining the particles breakup term due to bubble bursting[32] and the PSG method,[24] and the validity of the numerical calculation method was demonstrated by comparing the numerical results with the experimental ones.

## 2. Theoretical Analysis

### 2.1. Agglomeration Model

The following equations express the population balance equation[15,24] and collision frequency function[16,31] between two particles for calculating the temporal change in the number of agglomerated particles.

$$\frac{\mathrm{d}N_k}{\mathrm{d}t}=\frac{1}{2}\sum_{i=1,i+j=k}^{k-1}\left(1+\delta_{ij}\right)\alpha\left(a_i,a_j\right)N_iN_j-\sum_{i=1}^{M}\alpha\left(a_i,a_k\right)N_iN_k \quad \text{..... (1)}$$

$$\alpha\left(a_i,a_j\right)=1.3Z\left(a_i+a_j\right)^3\left(\frac{\varepsilon}{\nu}\right)^{\frac{1}{2}} \quad \text{..... (2)}$$

$$Z=0.727\left[\frac{\mu a_{\mathrm{Mo}}{}^3\left(\frac{\varepsilon}{\nu}\right)^{\frac{1}{2}}}{A_{131}}\right]^{-0.242} \quad \text{..... (3)}$$

Here, $N_i$: number density of clusters of i-particles, $a_i$: volumetric equivalent radius of a cluster of $i$-particles [m], $\delta_{ij}$: Klonecker's delta function ($\delta_{ij}=1$ for $i=j$, $\delta_{ij}=1$ for $i\neq j$), $\alpha(a_i, a_j)$: collision frequency function [m$^3$/s] of clusters of $i$- and $j$- group particles, $M$: largest number [-] of agglomerated particles, $\varepsilon$: dissipation rate of turbulence energy [m$^2$/s$^3$], $\nu$: kinetic viscosity [m$^2$/s], $Z$: corrected term [-] considering the effect of the London-van der Waals force based on liquid viscosity, $\mu$: viscosity [Pa·s], $a_{\mathrm{Mo}}$: Modal radius of the initial particles [m], and $A_{131}$: Hamarker constant [J], where the suffix 1 means particle and 3 means liquid. Here, $a_1=1.0$ $\mu$m was used in Eq. (3) because it was the minimum radius of polydisperse particle used for the experiment described in Chapter 3.

The agglomeration behavior of the particles with a primary size distribution requires a different approach from that used with particles having an equal initial particle radius because the equivalent radius and number of agglomerated particles do not have a one-to-one correspondence. The PSG method for calculating the agglomeration of size-distributed primary particles developed by Nakaoka *et al.*[24] is a new methodology to reduce the computation load. As shown schematically in **Fig. 1**, the clusters of agglomerated particles are divided into $M$ groups with characteristic radii of $a_1$, $a_2$, ..., $a_{\mathrm{M}}$ so as to maintain the volume ratio $R_{\mathrm{v}}$ [-] of adjoining characteristic particles.

$$R_{\mathrm{v}}=\frac{V_k}{V_{k-1}} \quad \text{..... (4)}$$

$$V_k=\frac{4}{3}\pi a_k{}^3 \quad \text{..... (5)}$$

Here, $V_{\mathrm{k}}$: characteristic volume of group $k$ defined by Eq. (5).

Therefore, the normalized population balance equation for group $k$ particles is expressed as follows:

$$\frac{\mathrm{d}N_k^*}{\mathrm{d}t^*}=\sum_{i=i_{c,k-1}}^{k-1}\xi_{i,k-1}\left(a_i^*+a_{k-1}^*\right)^3N_i^*N_{k-1}^*+\sum_{i=1}^{i_{c,k-1}}\zeta_{i,k}\left(a_i^*+a_k^*\right)^3N_i^*N_k^*-\sum_{i=i_{c,k}}^{M-1}\left(1+\delta_{ij}\right)\left(a_i^*+a_k^*\right)^3N_i^*N_k^* \quad \text{..... (6)}$$

$$t^*=1.3Za_{\mathrm{Mo}}{}^3\left(\frac{\varepsilon}{\nu}\right)^{\frac{1}{2}}N_0t \quad \text{..... (7)}$$

$$\xi_{i,k-1}=\frac{\left(V_i+V_{k-1}\right)}{V_k} \quad \text{..... (8)}$$

$$\zeta_{i,k}=\frac{V_i}{V_k} \quad \text{..... (9)}$$

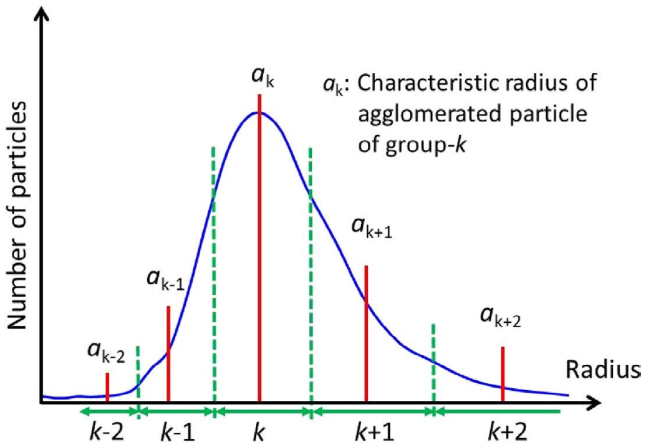


**Fig. 1.** Schematic image of distributed particle grouping in Particle-Size-Grouping (PSG) method. (Online version in color.)

Here, $N_k^*$: normalized number density of group $k$ particles ($=N_k/N_0$), $N_0$: initial number density [$m^{-3}$] of primary particles, $M$: maximum size number [-], $t^*$: normalized time defined by Eq. (7), $a_i^*$: normalized characteristic radius [-] of group $k$ particles ($=a_i/a_{Mo}$), $i_{c,k-1}$: critical size number [-] and $\xi_{i,k-1}$, $\zeta_{i,k}$: correction factors [-] for the particle number density to maintain the conservation of particle volume, as defined by Eqs. (8) and (9), respectively.

### 2.2. Breakup Term of Agglomerated Particles

Sumitomo *et al.*[32] imagined that the agglomerated particles adhering to a bubble surface are partially broken up at the liquid free surface during bubble bursting, as shown schematically in **Fig. 2**, and developed a mathematical breakup model for agglomerated particles with a single primary size (monodisperse particles). In the present study, a modified breakup model for initial particles with a size distribution (polydisperse particles) was developed for extension to the PSG method. The breakup term is given by Eq. (10).

$$\frac{dN_k}{dt} = \sum_{i=k+1}^{M} \beta\chi_{k|i}\omega\left(a_i, \frac{d_B}{2}\right)N_i N_B + \frac{N_k}{N_k + N_{k-1}}\beta\chi_{k|k+1}\omega\left(a_{k+1}, \frac{d_B}{2}\right)N_{k+1}N_B - \left\{\beta\omega\left(a_k, \frac{d_B}{2}\right)N_k N_B - (1-\beta)\omega\left(a_k, \frac{d_B}{2}\right)N_k N_B\right\} \quad \text{... (10)}$$

Here, $\beta$: decomposed ratio of the agglomerated particles of group $k$ below group $k$, $\omega\left(a_i, \frac{d_B}{2}\right)$: breakup frequency function by bubble bursting, $\chi_{k|i}$: breakup distribution function [-] defined as the volumetric ratio of group $k$ particles obtained from the breakup of group $i$ particles, $d_B$: diameter [m] of a gas bubble and $N_B$: number density [$m^{-3}$] of gas bubbles. The first term of the right-hand side in Eq. (10) indicates the formation number of group $k$ due to the breakup of agglomerated particles above group $k+1$. As group $k+1$ is divided into groups $k$ and $k$, and groups $k$ and $k$-1, the second term in Eq. (10) is necessary for additional formation number of group $k$ due to groups $k$ and $k$. The third and fourth terms in Eq. (10) represent conditions in which the agglomerated particles of group $k$ decompose below group $k$ at a rate of $\beta$ or remain in the same group, respectively.

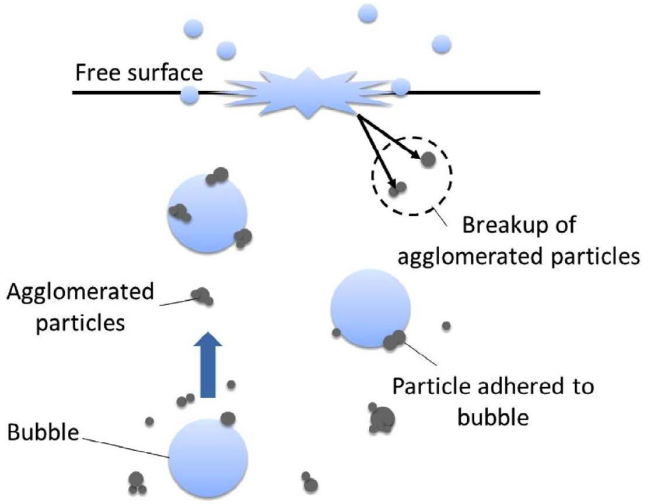


**Fig. 2.** Schematic image of adhesion of agglomerated particles to bubble surface and their breakup due to bubble bursting. (Online version in color.)

Assuming that $\omega\left(a_i, \frac{d_B}{2}\right)$ is composed of the product of two items: one is the frequency function, $\gamma$ [$m^3/s$], of particles adherence to bubbles and the other is the breakup efficiency, $\delta$ [-], of adhering particles at the bubble bursting,[32] the following equation is given

$$\omega\left(a_i, \frac{d_B}{2}\right) = \gamma \cdot \delta \quad \text{... (11)}$$

Here, the $\gamma$ item introduced by Arai *et al.*[35] was given by Eq. (12), and $\delta$ was expressed as the function of non-dimensional particle number, bubble diameter and bubble number[32] so as to obtain the constant parameter, $K$, by Eq. (13).

$$\gamma = \pi\left(a_i + \frac{d_B}{2}\right)^2 u_B \cdot A\left(\frac{2a_i}{d_B}\right)\varepsilon^{-B}\frac{1}{1+\exp\left[-L\left(\theta-\theta_i\right)\right]} \quad \text{... (12)}$$

$$\delta = K \cdot \left(\frac{d_B}{2a_{Mo}}\right)^5 \left(\frac{N_B}{N_{t0}}\right)^2 \quad \text{... (13)}$$

where $u_B$ is bubble floating velocity [m/s], $\theta$ is contact angle, $A$(=0.57), $B$(=0.21), $L$(=3.5) and $\theta_i$(=88) are constant, and $K$ becomes 150.[32]

As group $i$ particles splits into two groups in $i$-1 ways, $\chi_{k|i}$ is assumed to be expressed by Eq. (14).[32]

$$\chi_{k|i} = \frac{1}{i-1} \quad \text{... (14)}$$

Substituting Eqs. (11)–(14) into Eq. (10), the following equation is obtained as a non-dimensional form.

$$\frac{dN_k^*}{dt^*} = \sum_{i=k+1}^{M} S\beta\chi_{k|i}\left(a_i^* + \frac{d_B^*}{2}\right)^2 N_i^* N_B^* + \frac{N_k^*}{N_k^* + N_{k+1}^*}S\beta\chi_{k|k+1}\left(a_k^* + \frac{d_B^*}{2}\right)^2 N_{k+1}^* N_B^* - \left\{S\beta\left(a_k^* + \frac{d_B^*}{2}\right)^2 N_k^* N_B^* - S(1-\beta)\left(a_k^* + \frac{d_B^*}{2}\right)^2 N_k^* N_B^*\right\} \quad \text{... (15)}$$

$$S = 51.6 \cdot \frac{d_B^4 N_B^2 u_B \nu^{0.5}}{a_{Mo}^5 N_0^2 Z\varepsilon^{0.71}} \cdot \frac{1}{1+\exp\left[-L\left(\theta-\theta_i\right)\right]} \quad \text{... (16)}$$

where $N_B^*$ and $d_B^*$ are normalized number density ($=N_B/N_0$) and diameter ($=d_B/a_{Mo}$) of gas bubbles, respectively.

### 2.3. Combination of Particle Agglomeration and Breakup by PSG Method and Calculation Conditions

The population balance equation of particle agglomeration and breakup using the PSG method is expressed by Eq. (17).

$$\frac{dN_k^*}{dt^*} = \sum_{i=i_{c,k-1}}^{k-1} \xi_{i,k-1}\left(a_i^* + a_{k-1}^*\right)^3 N_i^* N_{k-1}^* + \sum_{i=1}^{i_{c,k-1}} \zeta_{i,k}\left(a_i^* + a_k^*\right)^3 N_i^* N_k^* - \sum_{i=i_{c,k}}^{M-1}\left(1+\delta_{ij}\right)\left(a_i^* + a_k^*\right)^3 N_i^* N_k^* + \sum_{i=k+1}^{M} S\beta\chi_{k|i}\left(a_k^* + \frac{d_B^*}{2}\right)^2 N_i^* N_B^* + \frac{N_k^*}{N_k^* + N_{k+1}^*} S\beta\chi_{k|k+1}\left(a_k^* + \frac{d_B^*}{2}\right)^2 N_{k+1}^* N_B^* - \left\{ S\beta\left(a_k^* + \frac{d_B^*}{2}\right)^2 N_k^* N_B^* - S(1-\beta)\left(a_k^* + \frac{d_B^*}{2}\right)^2 N_k^* N_B^* \right\} \quad \text{..... (17)}$$

The experimental size distribution curves of the primary particles ($t$ = 0 min in **Fig. 5**) was used for the initial particle condition. The values of $a_1$, $M$, and $\beta$ were set to 1.0 $\mu$m, 20, and 0.9, respectively. The $\beta$ value was determined to best fit the calculated temporal changes in particles agglomeration into experimental ones. The values of $d_B$ and $N_B$ were calculated by the procedure proposed by Sumitomo *et al.*[32] as shown in **Table 1**. The temporal change of Eq. (17) was calculated numerically by the Runge-Kutta method with the time step $\Delta t^*$ of $10^{-5}$ s.

The schematic image of inflow and outflow of group $k$ particles by agglomeration and breakup is shown in **Fig. 3**. As the $i_{c,k-1}$ in Eq. (17) became $k$-2 in the case of $R_V$=2,[24] the group $k$ particles are formed by agglomeration between group $k$-1 and group $k$-2 or $k$-1, and by breakup between group $k$+1 and group $k$ or $k$-1. These particles sometimes remain in the same group by agglomeration and breakup of fine particles. Meanwhile, the group $k$ particles are separated from the group $k$ by the breakup between group $k$ and group $k$-1 or $k$-2, and by the agglomeration between group $k$ and group $k$ or $k$-1.

**Table 1.** Calculation conditions of gas stirring.

| | 1.5 L/min (STP) | 2.0 L/min (STP) | 2.0 L/min (STP) |
|---|---|---|---|
| $N_B$ [m$^{-3}$] | 1 655 | 1 649 | 1 639 |
| $d_B$ [m] | 0.0124 | 0.0135 | 0.0144 |

## 3. Experiment

A schematic diagram of the experimental apparatuses and their dimensions for (a) impeller stirring and (b) gas stirring are shown in **Fig. 4**. The size of the acrylic cylindrical vessel (vessel inner diameter: 0.12 m, water depth: 0.13 m) used in the experiment was the same for both stirring processes. The paddle-type impeller (blade diameter: 0.05 m, thickness: 0.02 m, number of blades: 2) and nozzle tip (inner diameter: 0.005 m) used to introduce the stirring gas were set at the same immersion depth of 0.08 m from the free surface, as shown in Fig. 4.

The physical properties of the particles and liquid are shown in **Table 2**. Polydisperse PMMA particles (MZ-10HN, Soken Chemical & Engineering Co., Ltd.) having a modal diameter of 7.8 × $10^{-6}$ m were used for as the model particles, whereas the modal diameter of the monodisperse PMMA particles (MX-1000, Soken Chemical & Engineering Co., Ltd.) was 9.0 × $10^{-6}$ m. The PMMA density and Hamarker constant for the numerical calculation were 1.20 × $10^3$ kg/m$^3$ and 1.05 × $10^{-20}$ J, respectively. A 3.0 kmol/m$^3$ KCl solution was used for the rapid agglomeration condition, as this solution forms a thinner electric double layer around the particles and causes negligible repulsion between particles. The liquid density and viscosity were 1.13 × $10^3$ kg/m$^3$ and 9.27 × $10^{-4}$ Pa·s, respectively. A given number of PMMA particles was put into a small amount of ion-exchanged water and thoroughly dispersed with an ultrasonic cleaner (Series 8500, Branson). The experiment started when the water containing the particles was charged into the KCl solution. 1.0×$10^{-6}$ m$^3$ of the particle-suspended liquid was taken in a single sampling, and the sampling point was fixed at a position 0.02 m from the center axis of the vessel and 0.05 m above the vessel bottom. The sampling times were 0, 2, 5, 10, 30, 60, 120 and

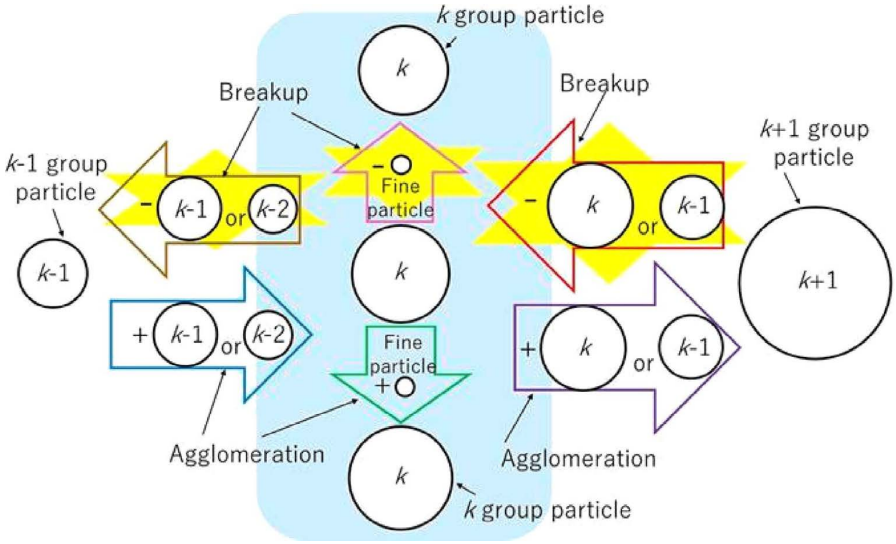


**Fig. 3.** Schematic image of inflow and outflow of $k$ group particles by agglomeration and breakup. (Online version in color.)

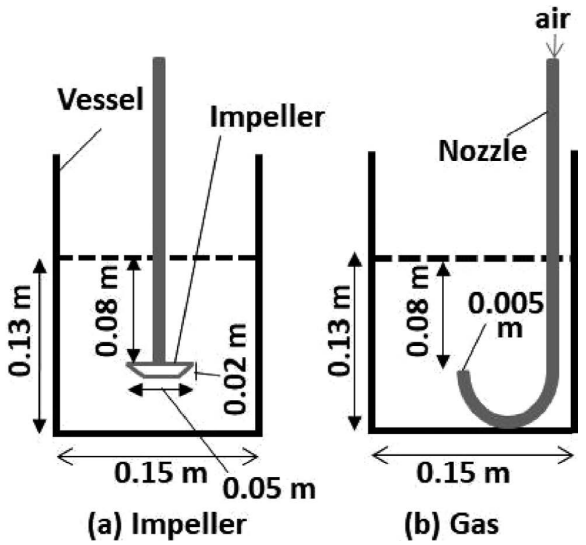


**Fig. 4.** Schematic diagram of experimental apparatuses for (a) impeller stirring and (b) gas stirring and their dimensions.

**Table 2.** Physical properties of particles and liquid used in experiment.

| Phase | Property | | |
|---|---|---|---|
| PMMA particle | Modal diameter (m) | Polydisperse | $7.8\times10^{-6}$ |
| | | Monodisperse | $9.0\times10^{-6}$ |
| | Density, $\rho_P$ (kg/m$^3$) | | $1.20\times10^{3}$ |
| | Hamaker constant, $A_{131}$ (J) | | $1.05\times10^{-20}$ |
| Liquid | KCl concentration (mol/m$^3$) | | $3.0\times10^{3}$ |
| | Density, $\rho_L$ (kg/m$^3$) | | $1.13\times10^{3}$ |
| | Viscosity, $\mu$ (Pa s) | | $9.27\times10^{-4}$ |

**Table 3.** Experimental conditions and equal energy input rate into liquid.

| | Energy input rate | $\varepsilon$ (W/kg) | 0.021 | 0.027 | 0.035 |
|---|---|---|---|---|---|
| Impeller | Rotation speed | $R$ (rpm) | 250 | 275 | 300 |
| Gas | Gas flowrate | $Q$ (L/min (STP)) | 1.5 | 2.0 | 2.5 |

180 min. The temporal changes in the number of agglomerated particles and their size distribution were measured by a particle size distribution analyzer (Multisizer 3, Beckman Coulter Inc.). The particle size measured here was the volume-equivalent diameter. The initial total number densities of polydisperse and monodisperse particles in the KCl solution were $1.5\times10^{9}-2.3\times10^{9}$ and $1.8\times10^{9}-2.0\times10^{9}$ m$^{-3}$, respectively.

**Table 3** shows the operating variables for the impeller and gas stirring processes and their values at an equal energy input rate calculated by Sumitomo *et al.*[32] The rotation speed of the impeller was varied to 250, 275 and 300 rpm and the gas flowrate was changed to 1.5, 2.0 and 2.5 L/min (STP), corresponding to energy input rates of 0.021, 0.027 and 0.035 W/kg, respectively.

## 4. Results and Discussion

### 4.1. Temporal Changes in Size Distribution and Number of Particles in Impeller and Gas Stirring

Figure 5 shows the comparison of the temporal changes in the particle diameter distributions under impeller stirring (Figs. 5(a) and 5(c)) and gas stirring ((b) and (d)), and in stirring of polydisperse particles ((a) and (b)) and monodisperse particles ((c) and (d)). The energy input rate for both stirring operations was fixed at 0.027 W/kg, that is, the impeller speed of 275 rpm and gas flowrate of 2.0 L/min (STP), as indicated in Table 3. From Figs. 5(a) and 5(b), the peak of the polydisperse particles decreased and the ratio of larger particle size increased slightly with increasing time in both impeller and gas stirring, while the sharp peak of the monodisperse particles in Figs. 5(c) and 5(d) also decreased as time proceeded, and a second peak, which indicates a cluster of 2 particles, appeared due to the agglomeration of the monodisperse particles. Comparing impeller stirring ((a) and (c)) and gas stirring ((b) and (d)), the peak values for impeller stirring showed larger decreases than those for gas stirring with both polydisperse and monodisperse particles. In the case of gas stirring, the peak for the polydisperse particles was almost unchanged after 60 min, as seen in Fig. 5(b). Larger second peaks of the monodisperse particles were observed with impeller stirring compared with gas stirring, as seen in Fig. 5(c).

The temporal changes in the total number $N_t$ [-] of particles normalized by the initial number of non-agglomerated particles $N_0$ [-] are shown in **Fig. 6**. Figures 6(a), 6(b) and 6(c) indicate the results for the polydisperse particles and (d) shows the results for the monodisperse particles. Here, the same energy input rate (0.027 W/kg) is used in Figs. 6(b) and 6(d). The number of particles decreased with increasing time in both impeller and gas stirring; that is, particle agglomeration progressed during the experiment. As seen in Figs. 6(a), 6(b) and 6(c), the agglomeration rate of the polydisperse particles under impeller stirring increased at higher rotation speeds, and the agglomeration rate was more rapid than that under gas stirring except the first half period of Fig. 6(a), whereas the agglomeration rate under gas stirring obviously decreased with an increasing gas flowrate. As enhancement of the energy input rate increases turbulent coagulation,[31] which promotes particle agglomeration, breakup of the agglomerated particles must be introduced in the case of gas stirring, as indicated in Chapter 2.

As seen in Fig. 6(d), the agglomeration rate of monodisperse particles (modal diameter: 9.0 $\mu$m) for impeller stirring was slightly larger than that for the gas stirring. The difference of the polydisperse particle agglomeration rate (Fig. 6(b)) in impeller and gas stirring was larger than the agglomeration rate of the monodisperse particles (Fig. 6(d)), even though the modal diameters were similar. This means that agglomerated polydisperse particles with different primary particle sizes break up more easily as a result of gas bubble bursting than monodisperse particles, which have the same primary size. This difference can be explained by the weaker bond force between size-distributed particles.

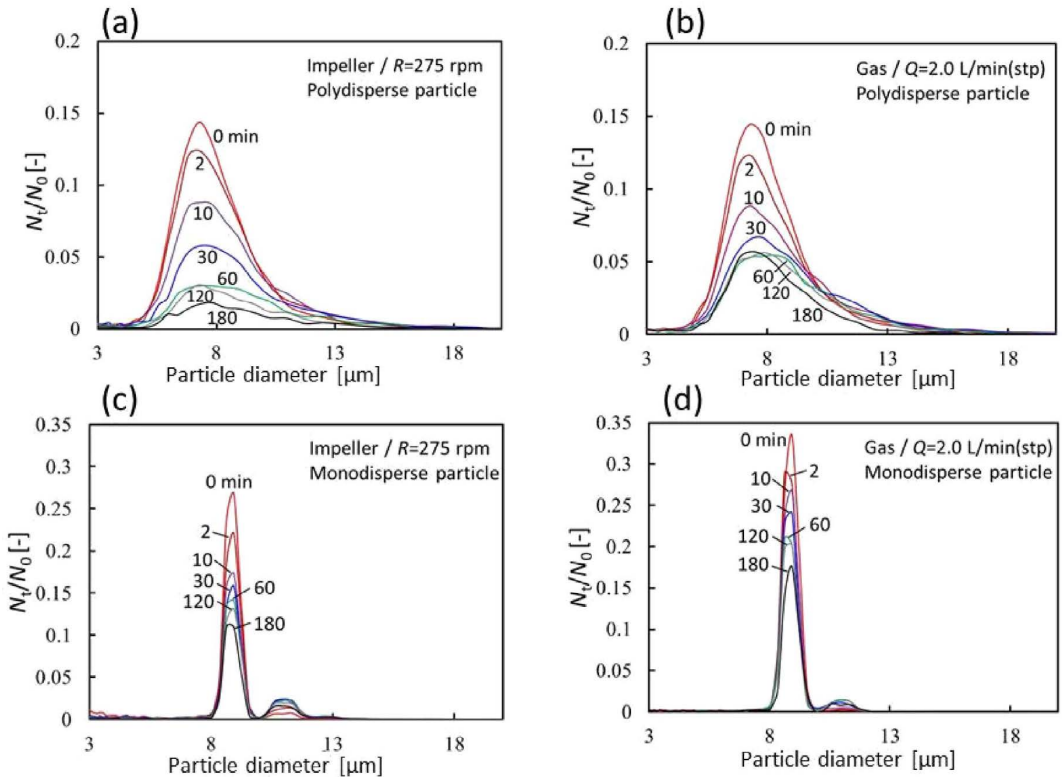


**Fig. 5.** Comparison of temporal changes in particle size distribution in impeller stirring and gas stirring at equal energy input rate ($\varepsilon$ = 0.027 W/kg). (Online version in color.)

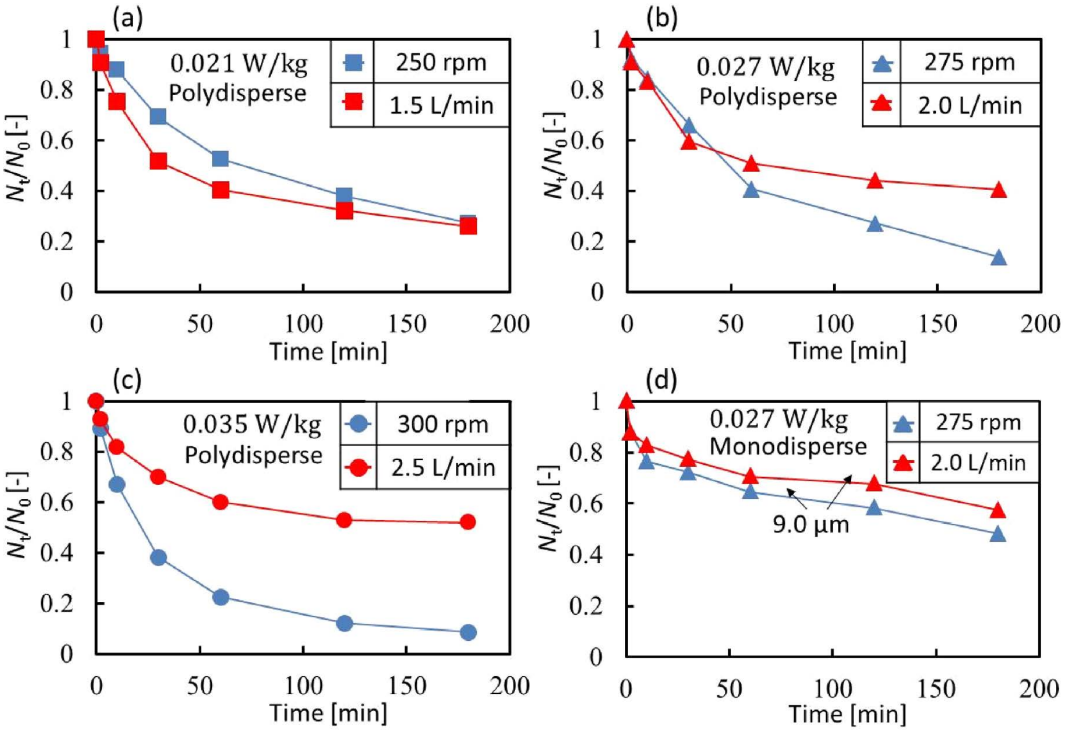


**Fig. 6.** Comparison of temporal changes in number of particles in impeller stirring and gas stirring. (Online version in color.)

### 4.2. Comparison of Numerical and Experimental Results for Agglomeration Behaviors under Impeller and Gas Stirring

A comparison of the experimental and calculated temporal changes in the number of particles is shown in **Fig. 7** for impeller stirring and in **Fig. 8** for gas stirring. In these figures, (a), (b) and (c) show the results for the polydisperse particles and (d) shows the results for the monodisperse particles. In the case of the polydisperse particles, the numerical changes in the number of particles with time was in good agreement with the experimental results in all cases. The numerical agglomeration curves of the monodisperse par-

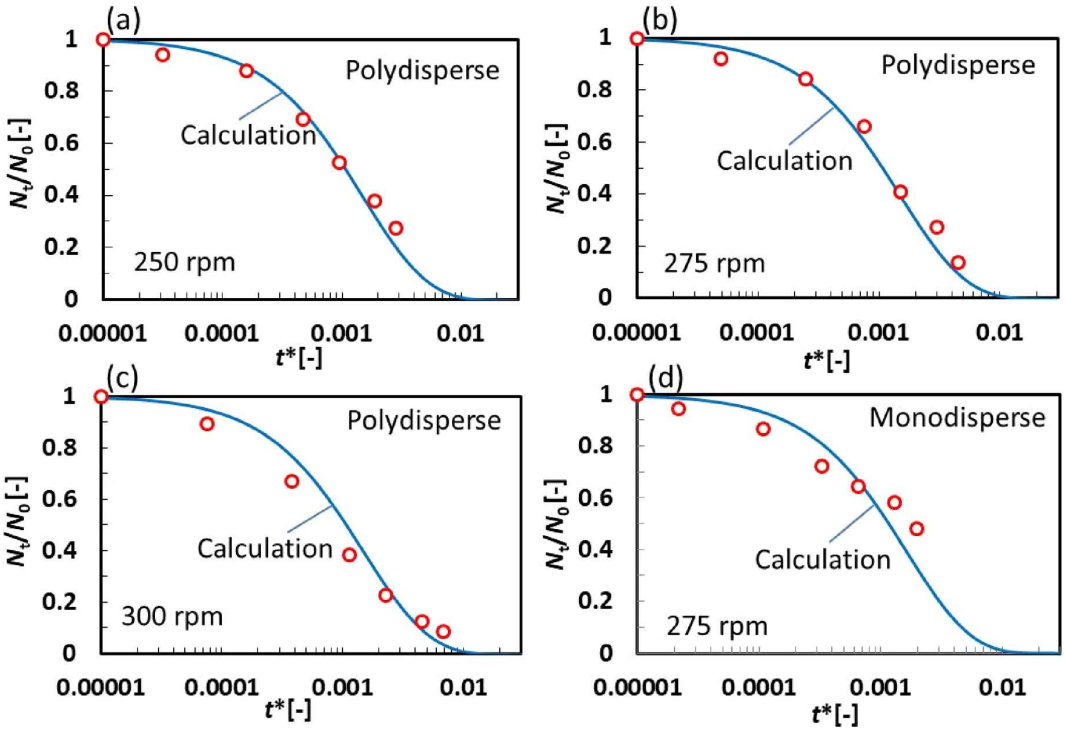


**Fig. 7.** Comparison of experimental and calculated temporal changes in number of particles in impeller stirring. (Online version in color.)

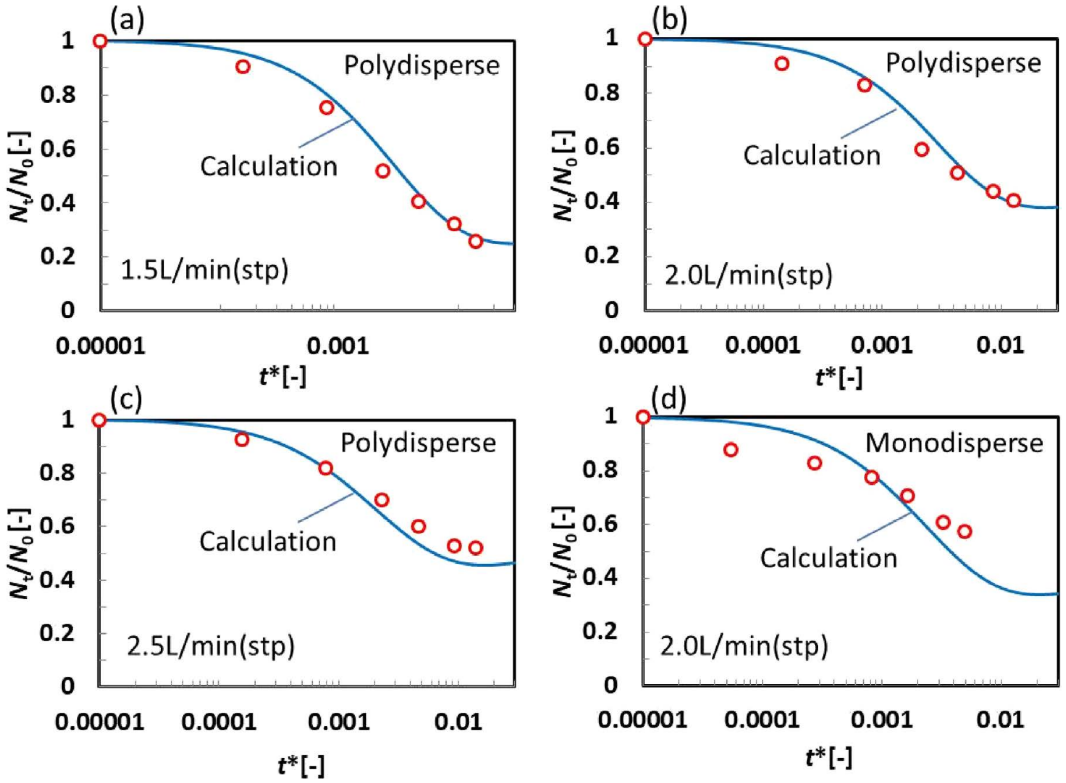


**Fig. 8.** Comparison of experimental and calculated temporal changes in number of particles in gas stirring. (Online version in color.)

ticles in (d) of Figs. 7 and 8 also explained the experimental plots, which indicates that the mathematical model in this study can be applied to the agglomeration behaviors of both polydisperse and monodisperse particles.

The experimental and calculated temporal changes in the number of group $k$ (G-$k$: $k$=3, 7, 9, 10) particles for impeller stirring are shown in **Fig. 9**. The polydisperse particles and rotation speed of 275 rpm were used here. The numerical curves showed good agreement with the experimental plots except for the mid-to-late period of G-9 and G-10.

The experimental and calculated results for the temporal changes in the number of group $k$ (G-$k$: $k$=3, 7, 9, 10) particles for gas stirring are compared in **Fig. 10**. The experimental and calculated results were in good agreement

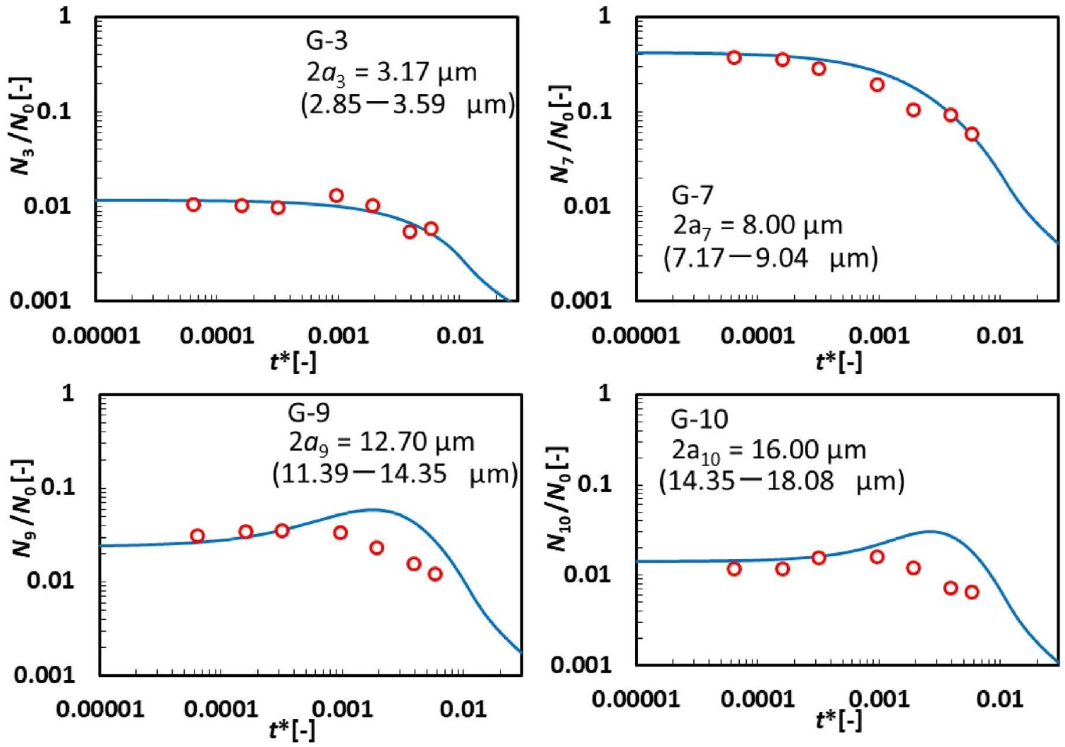


**Fig. 9.** Experimental and calculated temporal changes in number of group $k$ particles in impeller stirring (polydisperse particles, $R$ = 275 rpm). (Online version in color.)

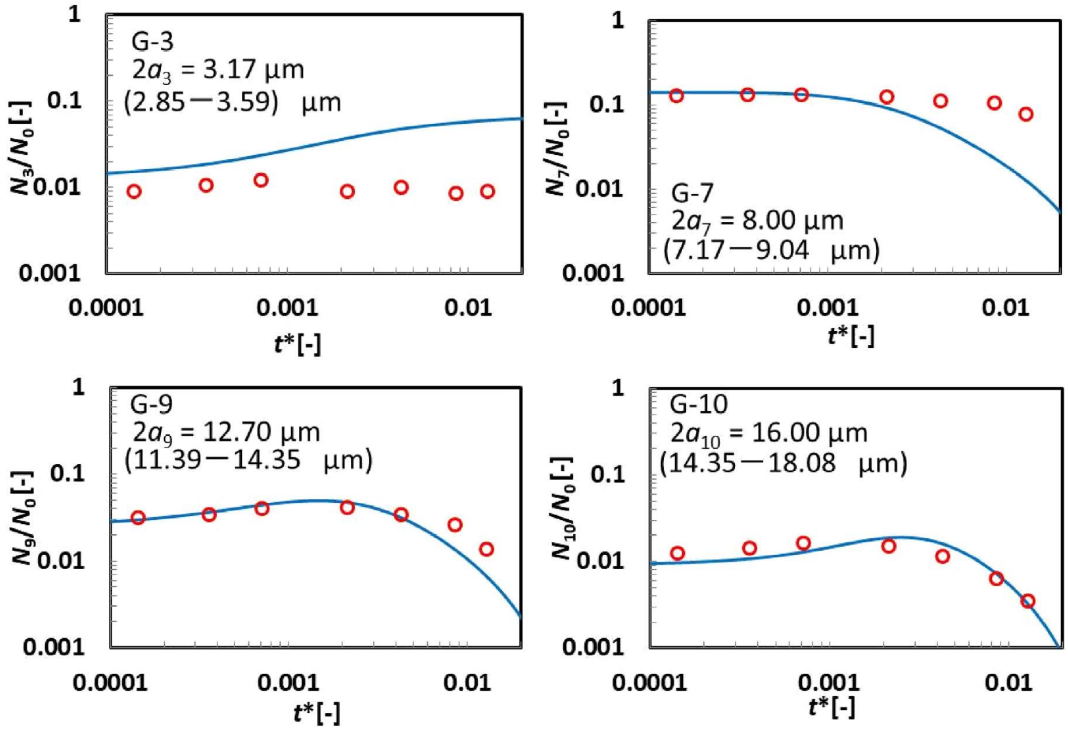


**Fig. 10.** Experimental and calculated temporal changes in number of group $k$ particles in gas stirring (polydisperse particles, $Q$ = 2.0 L/min (STP)). (Online version in color.)

for G-9 and G-10. However, the calculated agglomeration rate for G-3 was smaller than the experimental result due to the excess contribution of the breakup term, and acted in an opposite way in the mid-to-late period of G-7. This indicates that the assumption of the breakup term of agglomerated particles expressed by Eq. (12) should be improved, especially in the smaller group number, and is a subject for study in the next stage.

## 5. Conclusions

The agglomeration and breakup behaviors of polydisperse particles in a liquid under impeller stirring and gas stirring were compared by numerical calculations and model experiments. In the numerical agglomeration model of the particles, the PSG method was combined with a breakup term of agglomeration due to bubble bursting at the free surface.

(1) At an equal energy input rate, the agglomeration of polydisperse particles under impeller stirring was larger than that under gas stirring.

(2) The agglomeration rate of polydisperse particles under impeller stirring was promoted by an increasing energy input rate, whereas the agglomeration rate under the gas stirring decreased at higher energy inputs due to the larger contribution of breakup of the agglomerated particles during bubble bursting.

(3) At an equal energy input rate, the agglomeration rate of polydisperse particles was larger than that of monodisperse ones in both impeller and gas stirring, even though the modal diameters were similar.

(4) The computational changes in the total number of particles with time were in good agreement with the experimental results. This means that the difference in the agglomeration behaviors observed in impeller stirring and gas stirring can be explained by the turbulent coagulation and subsequent agglomerated particle breakup in gas stirring.

(5) The computational temporal changes in the number of particles of each group approximately agreed with the experimental results in both impeller and gas stirring.

## REFERENCES


1) K. Nakanishi and J. Szekely: *Trans. Iron Steel Inst. Jpn.*, **15** (1975), 522.
2) M. Söder, P. Jönsson and J. Alexis: *Scand. J. Metall.*, **31** (2002), 210.
3) D.-Y. Sheng, M. Söber, P. Jönsson and L. Jonsson: *Scand. J. Metall.*, **31** (2002), 134.
4) L. T. Wang, Q. Y. Zhang, S. H. Peng and Z. B. Li: *ISIJ Int.*, **45** (2005), 331.
5) K. Shirabe and J. Szekely: *Trans. Iron Steel Inst. Jpn.*, **23** (1983), 465.
6) Y. Miki, B. G. Thomas, A. Denissov and Y. Shimada: *Iron Steelmaker*, **24** (1997), 31.
7) O. J. Ilegbusi and J. Szekely: *ISIJ Int.*, **29** (1989), 1031.
8) A. K. Sinha and Y. Sahai: *ISIJ Int.*, **33** (1993), 556.
9) H. Tozawa, Y. Kato, K. Sorimachi and T. Nakanishi: *ISIJ Int.*, **39** (1999), 426.
10) Y. Miki and B. G. Thomas: *Metall. Mater. Trans. B*, **30** (1999), 639.
11) L. Zhang, S. Taniguchi and K. Cai: *Metall. Mater. Trans. B*, **31** (2000), 253.
12) H. Lei, B. Yang, Q. Bi, Y. Xiao, S. Chen and C. Ding: *ISIJ Int.*, **59** (2019), 1811.
13) L. Zhang, J. Aoki and B. G. Thomas: *Metall. Mater. Trans. B*, **37** (2006), 361.
14) U. Lindborg and K. Torssel: *Trans. Metall. Soc. AIME*, **242** (1968), 94.
15) M. V. Smoluchowski: *Z. Phys. Chem.*, **92** (1917), 129.
16) K. Higashitani, K. Yamauchi, Y. Matsuno and G. Hosokawa: *J. Chem. Eng. Jpn.*, **16** (1983), 299.
17) S. Taniguchi, A. Kikuchi, T. Ise and N. Shoji: *ISIJ Int.*, **36** (1996), S117.
18) M. Kobayashi and Y. Adachi: *Trans. Jpn. Soc. Irrig. Drain. Reclam. Eng.*, **191** (1997), 111.
19) H. Arai, Y. Nakamura, S. Shimasaki and S. Taniguchi: *Tetsu-to-Hagané*, **101** (2015), 129 (in Japanese).
20) H. Arai, Y. Nakamura, S. Shimasaki and S. Taniguchi: *Tetsu-to-Hagané*, **101** (2015), 139 (in Japanese).
21) M. Cerbelaud, A. Videcoq, P. Abélard, C. Pagnoux, F. Rossignol and R. Ferrando: *Langmuir*, **24** (2008), 3001.
22) M. Kobayashi: *J. Appl. Mech.*, **11** (2008), 517.
23) S. Rollié, H. Briesen and K. Sundmacher: *J. Colloid Interface Sci.*, **336** (2009), 551.
24) T. Nakaoka, S. Taniguchi, K. Matsumoto and S. Johansen: *ISIJ Int.*, **41** (2001), 1103.
25) T. Nakaoka: *Kobe Steel Eng. Rep.*, **56** (2006), 40.
26) H. Arai, H. Tsuchii and K. Matsumoto: *CAMP-ISIJ*, **31** (2018), 136, CD-ROM (in Japanese).
27) R. D. Vigil, I. Vermeersch and R. O. Fox: *J. Colloid Interface Sci.*, **302** (2006), 149.
28) T. Nakaoka, K. Matsumoto and S. Taniguchi: *Prog. Comput. Fluid Dyn.*, **8** (2008), 270.
29) S. T. Johansen and S. Taniguchi: Light Metals 1998, TMS, Warrendale, PA, (1998), 855.
30) S. Sumitomo, H. Koizumi, M. A. Uddin and Y. Kato: *Ultrason. Sonochem.*, **40** (2018), 822.
31) P. G. Saffman and J. S. Turner: *J. Fluid Mech.*, **1** (1956), 16.
32) S. Sumitomo, K. Yoshitomi, M. A. Uddin and Y. Kato: *ISIJ Int.*, **58** (2018), 1.
33) T. Murai, H. Matsuno, E. Sakurai and H. Kawashima: *Tetsu-to-Hagané*, **84** (1998), 13 (in Japanese).
34) K. Fuchigami, M. Wakoh, N. Imamura, K. Endoh, A. Kiyose and I. Sawada: *Tetsu-to-Hagané*, **85** (1999), 368 (in Japanese).
35) H. Arai, K. Matsumoto, S. Shimasaki and S. Taniguchi: *ISIJ Int.*, **49** (2009), 965.